PHYSICAL REVIEW C, VOLUME 61, 014603

Nuclear pion photoproduction in the Δ resonance region

D. Branford,[1] J. A. MacKenzie,[1] F. X. Lee,[5] J. Ahrens,[4] J. R. M. Annand,[2] R. Beck,[4] G. E. Cross,[2] T. Davinson,[1]
P. Grabmayr,[3] S. J. Hall,[2] P. D. Harty,[2] T. Hehl,[3] D. G. Johnstone,[1] J. D. Kellie,[2] T. Lamparter,[3] M. Liang,[1]
I. J. D. MacGregor,[2] J. C. McGeorge,[2] R. O. Owens,[2] M. Sauer,[3] R. Schneider,[3] A. C. Shotter,[1] K. Spaeth,[3] D. P. Watts,[2]
P. J. Woods,[1] L. E. Wright,[6] and T. T. Yau[2]
[1]*Department of Physics and Astronomy, University of Edinburgh, Edinburgh EH9 3JZ, Scotland*
[2]*Department of Physics and Astronomy, University of Glasgow, Glasgow G12 8QQ, Scotland*
[3]*Physikalische Institut, Universität Tübingen, D-72076 Tübingen, Germany*
[4]*Institut für Kernphysik, Johannes-Gutenberg Universität, D-55099 Mainz, Germany*
[5]*Department of Physics, George Washington University, Washington, DC 20052*
[6]*Department of Physics and Astronomy, Ohio University, Athens, Ohio 80309*

(Received 21 July 1999; published 16 December 1999)

A measurement of the $^{12}\mathrm{C}(\gamma,\pi^+n)^{11}\mathrm{B}$ reaction in quasifree π-production kinematic regimes has been performed using tagged photons in conjunction with large solid angle π and n detectors. The aim of the experiment was to investigate predicted modifications to the Δ excitation of nucleons and their subsequent propagation and decay, brought about by the nuclear medium. Differential cross sections are presented for photon energies spanning the Δ(1232) excitation region. The measurements are consistent with distorted wave impulse approximation calculations in which the amplitude for proton Δ excitation, followed by Δ propagation and decay to $\pi^+ + n$, is reduced compared to that for a free p. However, because of uncertainties in the magnitudes of the final state interactions, it is concluded that improved calculations are required to obtain a quantitative estimate of Δ-medium effects.

PACS number(s): 25.20.Lj, 13.60.Le, 13.60.Rj

INTRODUCTION

It is well known that excitation of the nucleon to the Δ(1232) resonance plays an important role in intermediate energy photonuclear reactions. However, although modifications to the excitation, propagation, and decay of the Δ, brought about by the surrounding nuclear medium, have been predicted (see, for example, Ref. [1]), few measurements against which to test these predictions have been made. Exclusive measurements of the $^{12}\mathrm{C}(\gamma,\pi^-p)^{11}\mathrm{C}$ and $^{16}\mathrm{O}(\gamma,\pi^-p)^{15}\mathrm{N}$ quasifree π-production reactions have been performed at Tomsk [2] and MIT-Bates [3], respectively. Both of these measurements sampled only a small region of the available phase space at photon energies of $E_\gamma = 380$ and 360 MeV, respectively. More recently, a high resolution study of the $^{16}\mathrm{O}(\gamma,\pi^-p)^{15}\mathrm{N}$ reaction has been reported from the National Institute voor Kernfysica en Hoge-Energiefysica, sectie K (NIKHEF-K) [4], and asymmetry measurements with polarized photons were carried out at Laser Electron Gamma Source (LEGS) [5]. Again, only small energy regions were studied, namely $E_\gamma \sim 360$ MeV and $E_\gamma = 293 \pm 20$ MeV, respectively. To provide a more comprehensive survey, we have made a measurement of the $^{12}\mathrm{C}(\gamma,\pi^+n)^{11}\mathrm{B}$ reaction using tagged photons covering a wide range of energies up to $E_\gamma \sim 400$ MeV. Furthermore, large position sensitive π and n detectors were employed so that angular distributions could be measured over a wide range of angles. The missing energy resolution was such that π production from the 1p shell could be separated from production involving the deeper 1s shell. Our aim was to provide data to test π-photoproduction models incorporating Δ-medium effects. The reasoning behind the measurement was that changes to the Δ mass and width will tend to redistribute the strength and this can only be seen when the reaction is studied over a wide range of energies and angles. A first report of some of the results of this experiment was presented in reference [6]. Here we present differential cross sections obtained from the full data set together with comparisons to new distorted wave impulse approximation (DWIA) calculations which permit investigations of Δ-medium effects to be made.

EXPERIMENTAL ARRANGEMENT

Figure 1 shows the experimental arrangement. A bremsstrahlung photon beam was produced by a ~ 15 nA beam of electrons from the Mainz microtron (MAMI-B) incident on a 4μm Ni radiator. The energies of photons in the range $E_\gamma = 114$–792 MeV were analyzed using the Glasgow tagging spectrometer [7,8]. The tagged photon resolutions and counting rates were typically $\Delta E_\gamma = 2$ MeV and $5 \times 10^7\ \mathrm{s}^{-1}$, respectively.

The photon beam was collimated to a diameter of 18 mm at the target, which was either 0.839 g cm^{-2} Carbon or 0.915 g cm^{-2} CH_2 inclined at an angle of 20° with respect to the beam direction. The fraction of tagged photons passing through the collimator, the tagging efficiency, was measured several times and remained stable at $55 \pm 1\%$. The energies and angles of particles produced in the target were measured by two large solid-angle detection systems. On one side of the beam, a plastic scintillator hodoscope (PiP) [9] was used to detect charged particles in the angular range $\theta = 50-130°$ and $\phi = (-24)$–24°. A time of flight detector array (TOF) was placed on the opposite side of the beam. This detector [10] consisted of six stands each containing 16 vertically mounted scintillators of dimension $3000 \times 200 \times 50$ mm in two ranks of 8 (see Fig. 1) and covered the range $\theta = 10$–150°. The range of azimuthal angles ϕ covered by

©1999 The American Physical Society

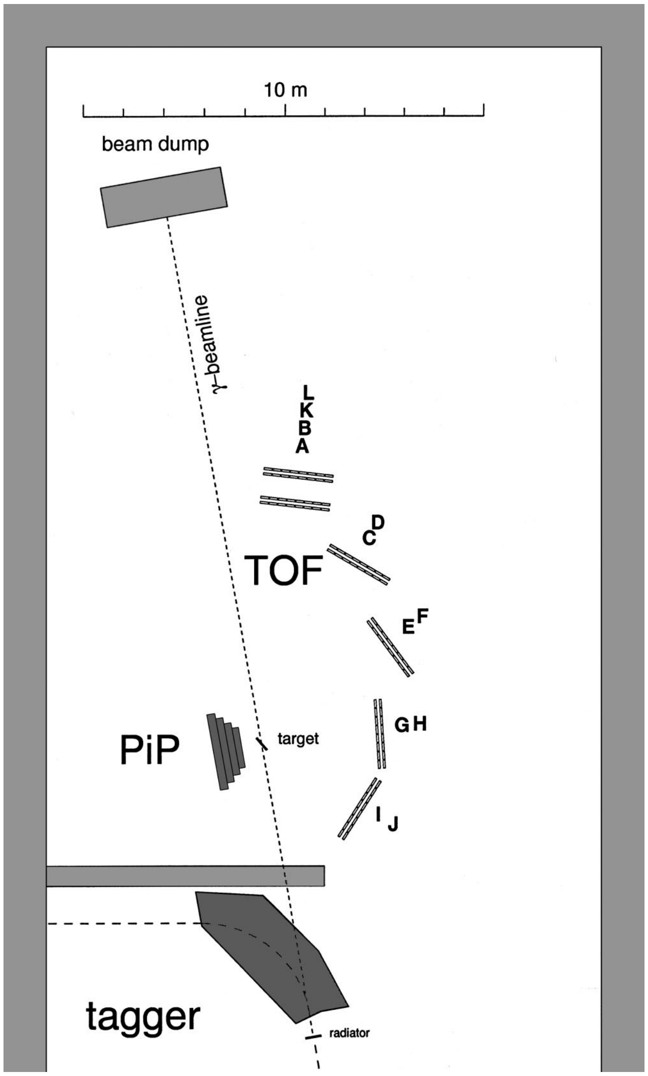

FIG. 1. Experimental arrangement used for the $^{12}\mathrm{C}(\gamma,\pi^{+}n)^{11}\mathrm{B}$ measurement.

each element depended on the distance from the target which was between 6 and 14 m. Surrounding the target at a radius of 11 cm was a ring of thin ΔE scintillator detectors, shown in Fig. 2, which had a dual purpose. Used in coincidence with PiP, they produced a trigger pulse for each detected charged particle. On the TOF side, the presence or absence of a signal in the appropriate element of this ring and a second half ring of detectors at 30 cm radius indicated a charged or neutral particle, respectively. The above system produced over 1000 channels of analog-to-digital converter (ADC) and time-to-digital converter (TDC) information which were read out using the ACQU data acquisition system [11].

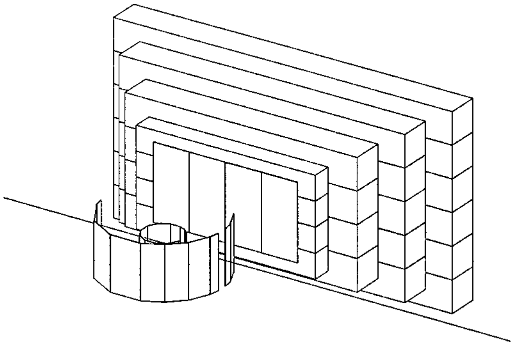

FIG. 2. Schematic diagram of the PiP detector showing the orientations of the thin ΔE detectors (vertical) and the thick E-detector bars (horizontal). Also shown is the ring and half ring of thin ΔE detectors with radii of 11 and 30 cm, respectively.

DETECTOR CALIBRATION AND DATA ANALYSIS

The main innovation of our measurement was the use of a plastic scintillator hodoscope to detect pions rather than a magnetic spectrometer, which is more conventional. This choice was made because magnetic spectrometers with sufficiently high resolution have too small an acceptance to allow a broad range measurement of the type described here. Since scintillator hodoscopes have not been used previously to detect pions with energies as high as those considered here, we describe the analysis in some detail.

Figure 2 shows a schematic of the PiP detector, which consisted of a 2 mm thick ΔE layer followed by four E layers of thickness 110, 175, 175, and 175 cm, all constructed from NE110 plastic scintillator material [9]. This gave a total stopping power of 180 MeV for pions entering normal to the detector. Events due to detecting π^{+} and π^{-} particles were separated from those due to protons and electrons by selecting a region of the $\Delta E-E$ distribution as shown in Fig. 3. It should be noted that the events shown in Fig. 3 all have an implicit afterpulse condition, discussed below, by virtue of the reaction trigger. This trigger condition removes the foldback in the π locus, which would otherwise be expected from high energy pions exiting the back of PiP, and also rejects high energy electrons, which would otherwise give signals that overlap with the π locus in Fig. 3. The electron and p regions evident in the figure are due to random coincidences with pulses that occur in the afterpulse inspect period. Events due to π^{+} particles were selected by demanding that an afterpulse occurred within the time interval 0.2–6.2 μs after the initial interaction. Since the $\pi^{+}\rightarrow\mu^{+}\rightarrow e^{+}$ decay chain is characterized by the 2.2 us decay constant of the μ^{+} decay, most π^{+} particles entering PiP give rise to afterpulses in the 6.0 μs inspection period. On

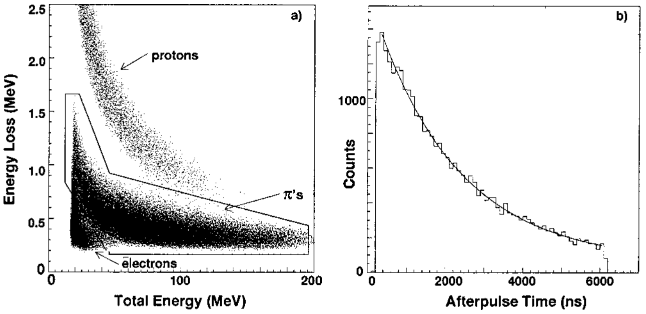

FIG. 3. (a) The ΔE-E plot showing the software window used for selecting events due to detecting pions. (b) Afterpulse time spectrum. The curve is a fit using the equation $y=p_1+p_2\exp(t/2190)$, where $p_1=63$ and $p_2=1540$.

the other hand, stopped π^- particles are quickly absorbed by nuclei releasing $\sim$140 MeV energy in typically a few ns, which is outside the accepted time region. Figure 3 also shows a typical decay curve which can be decomposed into the expected 2.2 μs decay curve and a flat background. The flat background gives the probability of particles entering the detector randomly within the 6.0 μs time interval. This was typically a few percent, which indicates that π^+ particles were identified with very little background contamination.

A simulation of the detector response made using the CERN library package GEANT [12] indicated that the largest background contamination arises from the decay $\pi^- \rightarrow \mu^-$ in flight. Typically, $\sim$8% of π^- particles emitted towards PiP decay in flight and satisfy the afterpulse requirements. However, events of this type are spread out over a wide energy range (typically 100 MeV) and are not generally expected to be in coincidence with an n observed in TOF. Hence, following application of missing energy and other conditions discussed later, the number of events expected from π^- decays in flight is $\lesssim 1\%$.

An undesirable property of this type of detector, which does not apply to magnetic spectrometers, is the degradation in resolution that occurs due to inelastic nuclear reactions in the scintillating material. However, the multilayer structure of the detector provides the means to reject most events of this type. Given that the problem is most serious for the higher energy pions, which traverse two, three, or four E layers of the detector, it is possible to demand in such cases that the energy deposited in each individual layer is consistent with purely electronic stopping. An algorithm to implement this condition was tested by considering a sample of pions from the $p(\gamma,\pi^+)n$ reaction obtained using the CH_2 target.

The above conditions determine the efficiency of PiP as a π^+ detector. In order to measure this efficiency, π^+ particles produced by the $p(\gamma,\pi^+ n)$ reaction in a CH_2 target, tagged by detecting the correlated n in TOF, were employed. By considering only E_γ, E_n, and θ_n, events from hydrogen could be selected. For each of these events, it was possible, using the kinematics of the reaction, to deduce the direction and energy of the corresponding π. The efficiency (ϵ_π) was obtained by comparing the number of tagged π^+ particles incident on the detector at a given energy and angle, to the number that actually survived to give an afterpulse and an energy consistent with the $p(\gamma,\pi^+ n)$ reaction. Figure 4(a) shows ϵ_π as a function of π energy. No angular dependence was observed within the accuracy of the measurement, which was $\pm 5\%$.

The n TOF technique is fairly standard and has been described elsewhere [13]. It was assumed a neutral (n or γ ray) had been detected when a signal occured in a TOF bar without a signal being present in the corresponding elements of the ΔE arrays surrounding the target. Events due to γ rays were discarded by making a cut on particle velocity. The energy dependence of the n detection efficiency is affected by the pulse height threshold and for the results reported here, we used a 5 MeV electron equivalent software cut. Figure 4b shows the corresponding efficiency (ϵ_n) calculated by the STANTON code [14] for one layer of TOF detectors. In general, two or four layers were employed as shown in Fig. 1 giving higher efficiencies.

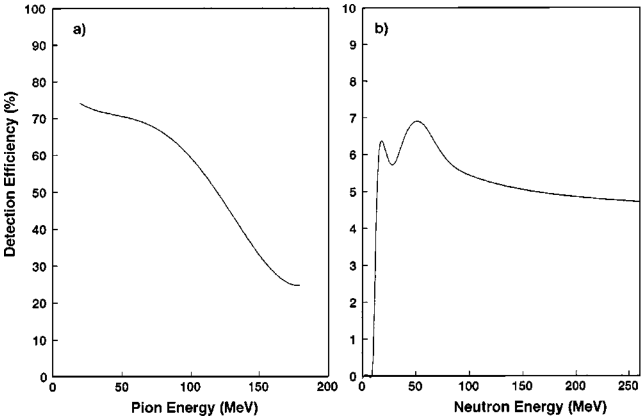

FIG. 4. (a) Experimentally determined π^+-detection efficiency ϵ_π versus E_π. (b) Neutron detection efficiency ϵ_n versus E_n calculated using the STANTON code.

In order to separate events corresponding to the removal of a p from the 1p and 1s shells of ^{12}C, it was necessary to obtain an overall energy resolution of better than 10 MeV. Hence, a good calibration of the various detectors was crucial. For PiP this was achieved using cosmic rays. Position information, derived from the time difference of signals arriving at the ends of each block, was used to determine the angle at which rays traversed PiP and thus produce an energy loss per unit path length spectrum for each block. These showed the expected Landau distribution and enabled an absolute energy calibration for each block to be obtained. Using these calibrations, the signals from the individual blocks were combined and the overall calibration thus obtained was checked later using the two body $p(\gamma,\pi^+ n)$ reaction.

Position calibration was achieved by selecting events in which charged particles from the target had traversed individual ΔE blocks, which acted as masks corresponding to known regions of the E blocks behind [9]. This procedure and its converse gave both a horizontal and vertical calibration in the detector frame of reference, which could then be transformed into the laboratory frame using the measured position and orientation of PiP.

The position of the TOF bars was surveyed using an ultrasonic distance meter. An energy versus pulse height calibration for each TOF bar was obtained from the Compton edges produced by 4.4 MeV (Am-Be) and 2.6 MeV (^{228}Th) γ rays, and from the maximum pulse height produced by protons which just stop in the bar. This maximum energy loss was estimated from the p stopping power to be 78 MeV. These calibrations were used to set the threshold which determines the n detection efficiency. The time of flight TDCs were calibrated using a pulser. The time peak produced by $v=c$ electrons and photons was used to obtain the true zero in the TDC spectra.

Each event recorded following a PiP trigger will generally contain output signals from more than one tagger focal plane detector and may contain more than one TOF detector signal. The contribution due to random coincidences was subtracted using the *weighted subevent* method. For this, prompt and

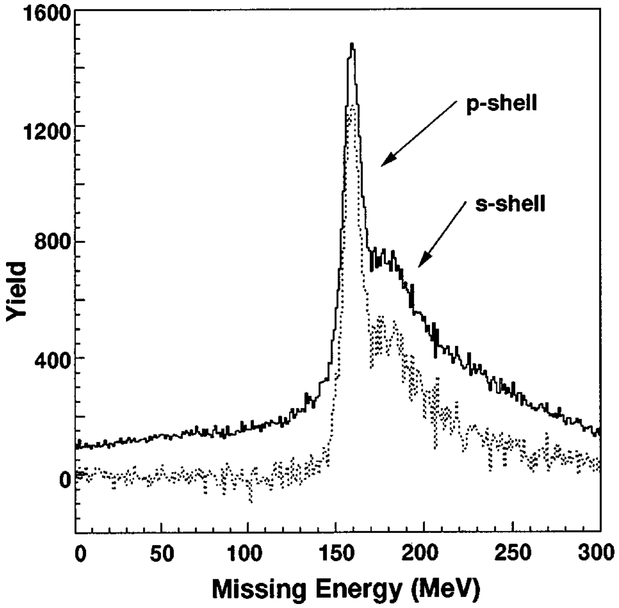

FIG. 5. Missing energy spectra for the ^{12}C$(\gamma,\pi^+n)^{11}$B reaction before (solid line), and after subtracting random backgrounds (dashed line).

random coincidence regions were defined in both the PiP-tagger and PiP-TOF time difference spectra. For each event, one selects hits in these regions of the time spectra and then constructs all subevents, i.e., all possible pairs of tagger and TOF hits. For each subevent, a tagger (or TOF) hit is given a weight $W_\gamma=+1(W_n=+1)$ if it is in the prompt region. If the hit is in the random region, the weight is negative and its magnitude is the ratio of the widths of the prompt and random regions.

Random afterpulses in PiP, which were generated by the detection of uncorrelated particles, were more difficult to deal with since they give rise to a flat background under an exponential curve in the delayed pulse TDC spectrum. The optimum solution in this case is to assign a weight, which changes steadily with the time of appearance of the afterpulse during the inspection period. However, this complexity was avoided in the present analysis. The decay spectrum was split into just two regions, the first being termed the pseudotrue region and the second, the pseudorandom. Appropriate weights W_π^{true} and W_π^{random}, which are positive and negative, respectively, were chosen so that the weighted sum of counts in the two regions gave the total number of delayed afterpulses [15]. The weight ascribed to a subevent is the product of the separate weights, $W_\gamma W_n W_\pi$. Each subevent is then analyzed independently and used in the accumulation of weighted spectra. This method avoids the need to generate four real and random data sets and subtract the resulting spectra.

Figure 5 shows the missing energy spectrum for the reaction ^{12}C$(\gamma,\pi^+n)^{11}$B with and without the randoms subtracted. The missing energy E_m is defined by the equation

$$E_m=E_\gamma-E_\pi-E_n-E_{recoil}=E_x-Q, \tag{1}$$

where E_γ is the energy of the tagged photon, E_π the kinetic energy of the π, E_n the kinetic energy of the n, and E_{recoil} the kinetic energy of the recoiling $A=11$ system determined using momentum conservation. E_x and Q are the excitation energy associated with the $A=11$ system and the Q value for the reaction leading to the ground state, respectively.

TABLE I. The binning regions used in extracting the ^{12}C$(\gamma,\pi^+n)^{11}$B cross sections.

Quantity	Range	Bin size	No. of bins
E_γ	240–400 MeV	40 MeV	4
E_π	20–180 MeV	10 MeV	16
θ_π	60–120°	15°	4
ϕ_π	(−15)–15°	30°	1
θ_n	10–150°	5°	28
$\phi_n-\phi_\pi$	170–190°	20°	1

As the aim of the experiment was to measure exclusive π^+ production on $1p$-shell nucleons, this channel was first isolated by applying a cut from E_m = 150–165 MeV in the missing energy spectrum. In order to obtain cross sections with a reasonable statistical accuracy, it was necessary to combine the data into fairly large energy and angle bins. The bins are noted in Table I. Yields (Y) for each bin were obtained using weights both to perform random subtractions and to compensate for the detection efficiencies according to the equations

$$Y=\sum_{events}\sum_{subevents}W, \tag{2}$$

$$W=\frac{W_\gamma W_\pi W_n}{\epsilon_\pi\epsilon_n}. \tag{3}$$

The statistical error in Y is given by

$$\sigma_Y=\left(\sum_{events}\sum_{subevents}W^2\right)^{1/2}. \tag{4}$$

Cross sections were extracted from these data using the equation

$$\frac{d^3\sigma}{d\Omega_\pi d\Omega_n dE_\pi}=\frac{Y\sin\theta_t}{n_t\phi_\gamma\Delta\Omega_\pi\Delta\Omega_n\Delta E_\pi}, \tag{5}$$

where θ_t is the target angle, n_t is the target density, ϕ_γ is the integrated tagged photon flux, $\Delta\Omega_\pi$ is the π solid angle, $\Delta\Omega_n$ is the n solid angle, and ΔE_π is the π energy range. The photon flux ϕ_γ was given by the number of electrons recorded in the tagger scalers multiplied by the tagging efficiency. Dead time was automatically corrected for by arranging so that the tagger scalers were disabled while the data acquisition system was busy.

The background due to photon interactions along the air path traversed by the photon beam was measured with the target removed. The target-out missing energy spectrum exhibited a small peak consistent with π^+ production on nitrogen and oxygen but the target-out yield was only ~2% of

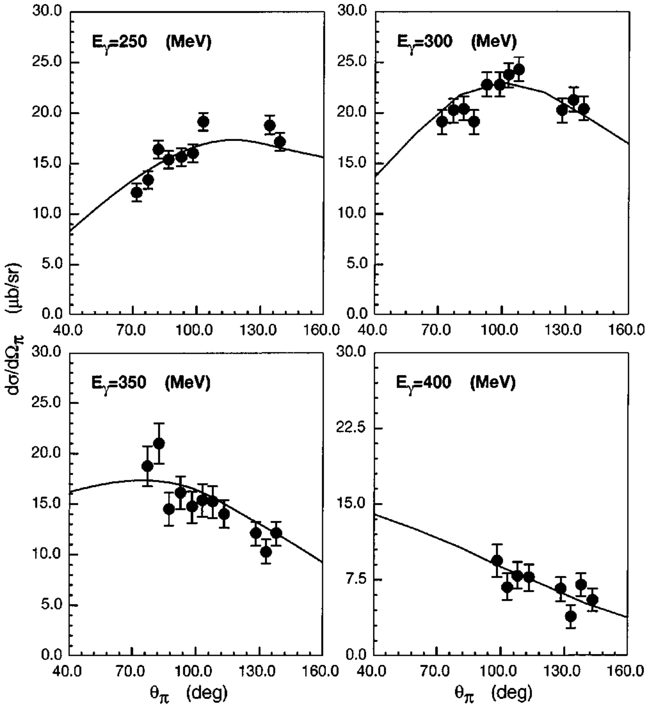

FIG. 6. Differential cross sections for the $p(\gamma,\pi^+n)$ reaction in the center of mass system. The curves were calculated using the theory of Blomqvist and Laget, which is known to describe well the previous experimental data. The data points from the present experiment have been increased in magnitude by a factor of 1.20.

the target-in yield. As this is well below the statistical and systematic uncertainties in the data, this background was neglected.

Results for the $p(\gamma,\pi^+n)$ reaction were obtained in a similar way using data taken with the CH_2 target. The $\gamma+p\rightarrow\pi^++n$ events were separated on the basis of their missing energy and the cross section was obtained by integrating over allowed E_π, θ_n, and ϕ_n. These cross sections are compared in Fig. 6 to calculations using the expressions of Blomqvist and Laget [16], which reproduce the previously measured cross sections [17] for this reaction. For this comparison, the calculated cross sections were averaged over the appropriate E_γ bins and detector acceptances. An overall normalization factor of 1.20 is required to bring the present $p(\gamma,\pi^+n)$ results into agreement with the calculations. Since this factor is consistent with the total systematic error of 20%, estimated from the uncertainties in target thickness, tagging efficiency, detector efficiencies, and solid angles, it was decided to renormalize the $^{12}C(\gamma,\pi^+n)^{11}B$ data by the same factor of 1.2. The systematic error of the renormalized $^{12}C(\gamma,\pi^+n)^{11}B$ data is obtained by combining the statistical errors of the present $p(\gamma,\pi^+n)$ data with the systematic errors of about ±4% for the previous data [17]. The resulting systematic error, ±10%, is significantly reduced compared to the systematic error of the present measurements taken alone.

RESULTS AND DISCUSSION

The missing energy distributions

The calibration of the system was checked by determining the missing energy spectrum for the $p(\gamma,\pi^+n)$ reaction. The spectrum obtained has a single peak with a centroid at $E_m=140.5\pm0.1$ MeV (statistical error only), which is consistent with the reaction Q value of 140.8 MeV and the ±1 MeV estimated systematic error in the missing energy determinations. The full width at half maximum (FWHM) resolution was $\Delta E_m=8.9$ MeV, which agrees well with an estimate obtained by adding in quadrature the resolutions $\Delta E_\gamma=2$ MeV, $\Delta E_\pi=7$ MeV, and $\Delta E_n=3.5$ MeV associated with the tagging system, PiP and TOF, respectively [15].

The large peak in the missing energy spectrum for the $^{12}C(\gamma,\pi^+n)^{11}B$ reaction shown in Fig. 5 occurs at 160 ± 0.1 MeV (statistical error only) and has a FWHM of $\Delta E_m\sim$ 12 MeV. There is an indication of a broader peak at $E_m\sim$ 180 MeV with $\Delta E_m\sim$ 25 MeV. Very similar spectra have been observed in the $^{12}C(e,e'p)^{11}B$ [18], $^{12}C(p,2p)^{11}B$ [19], and $^{12}C(p,d\pi^+)^{11}B$ [20] reactions. As in those cases, the two peaks are associated with removing protons from the $1p$ and $1s$ shell, respectively. A study of the $^{12}C(e,e'p)^{11}B$ reaction with high resolution showed strong excitation of the three low lying single-hole states in ^{11}B at $E_x=0.0$ MeV ($J^\pi=3/2^-$), 2.12 MeV ($1/2^-$), and 5.02 MeV ($3/2^-$) [21]. If the same three low-lying single hole states in ^{11}B are populated with similar intensities in the $^{12}C(\gamma,\pi^+n)^{11}B$ reaction, then folding in the experimental resolution would give a missing energy spectrum peaked at $E_m=160$ MeV with a width $\Delta E_m\sim$ 12 MeV, as is observed. In order to select events from the present $^{12}C(\gamma,\pi^+n)^{11}B$ data in which a $1p$ shell p is removed by quasifree knockout, a missing energy selection, $E_m=150$–165 MeV, was used as noted above. In the region of the 1s peak, a background not seen in the $^{12}C(e,e'p)^{11}B$ missing energy spectrum [18] is evident. This is probably due to nonquasifree processes or final state interactions (FSI), in which one or more of the final state particles go undetected. However, this background does not extend significantly into the $E_m=150$–165 MeV region since the thresholds for ^{11}B breakup to $^{10}B+n$ and $^{10}Be+p$ occur at $E_m=168.3$ and 168.0 MeV, respectively. Of greater concern is the experimental resolution, 8.9 MeV FWHM, as a result of which ~10% of the $1p$ removal events lie outside the selected $1p$ region and a similar proportion of 1s events fall within it. However, in view of the fact that calculations for $1p$ and $1s$ removal, averaged over our energy and angular bins, give roughly similar coincident n angular distributions [15,6,22], the n angular distributions considered below are not expected to be significantly distorted through contamination with $1s$ removal events. The events in the $1s$ peak region were not analyzed because the background under the peak is not sufficiently well understood.

Differential cross sections

Figures 7–8, which were obtained using the bins shown in Table I, show the θ_n dependence of the $1p$ removal cross sections for the $^{12}C(\gamma,\pi^+n)^{11}B$ reaction in the energy range $E_\gamma=240$–400 MeV for four θ_π bins. Figure 9 shows the photon energy dependence of the cross sections at the average θ_π angles 67°, 82°, 97°, and 112° obtained by integrating the results shown in Figs. 7–8 over the θ_n angles. Figure

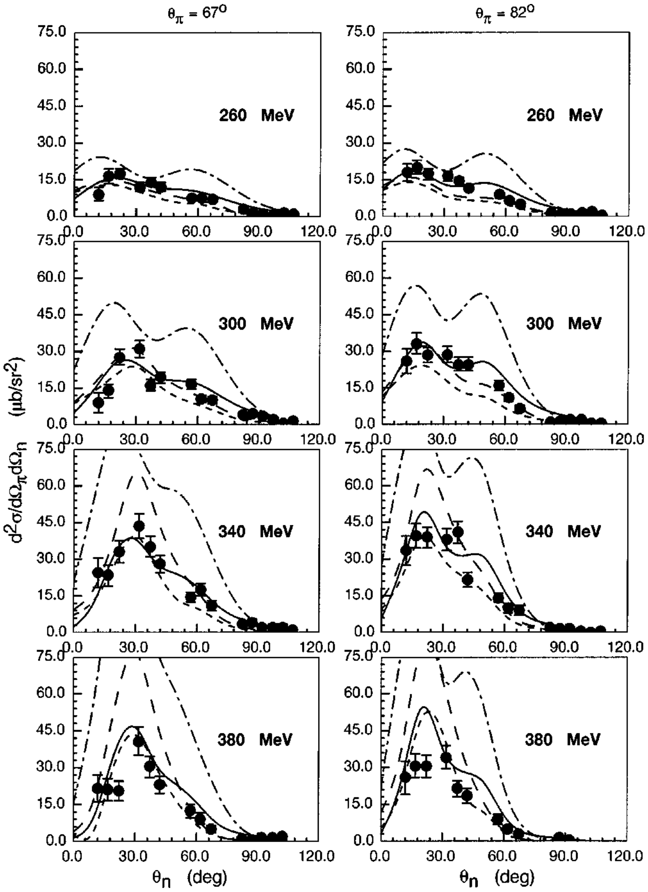

FIG. 7. Differential cross sections for the ^{12}C$(\gamma,\pi^+n)^{11}$B reaction versus n laboratory angle obtained at average π detection angles of $\theta_\pi = 67°$ and 82°, and average photon energies $E_\gamma = 260$, 300, 340, and 380 MeV. The E_γ, θ_π, ϕ_π, θ_n, and ϕ_n bins are as shown in Table I. The results are integrated over E_π and E_n. The theory curves are LWPW (dot dashed), LWDW (solid), VPW (long dashed), and VDW (dashed) calculations.

10 shows the E_π dependence of the cross sections at the average π angles $\theta_\pi = 67°$ and 112°. For these data, the θ_π and θ_n bins were 10° and 15° wide, respectively, and the θ_n bins were centered in each case around the θ_n angle at which the yield of neutrons from quasifree π^+ production is expected to be greatest. All the results show that the cross section is largest for $E_\gamma \sim 340$ MeV, which is consistent with a reaction proceeding through excitation of the $\Delta(1232$ MeV) resonance. In this E_γ region, the observed cross sections are comparable to ^{16}O$(\gamma,\pi^-p)^{15}$N cross sections at 360 MeV [3,4], which are interpreted in terms of quasifree π production including Δ excitation [3,4,23]. The outgoing nucleons from the ^{12}C$(\gamma,\pi^+n)^{11}$B and ^{16}O$(\gamma,\pi^-p)^{15}$N reactions have similar angular distributions and their variation with E_γ and θ_π is qualitatively as expected for quasifree π production. The angular range arises from the initial nucleon's Fermi motion. The variation in shape of the π energy spectrum in Fig. 10 can also be understood in terms of the quasifree kinematics. We conclude, therefore, that the ^{12}C$(\gamma,\pi^+n)^{11}$B results shown in Figs. 7–10 are consistent with a quasifree π^+ production process that involves Δ excitation.

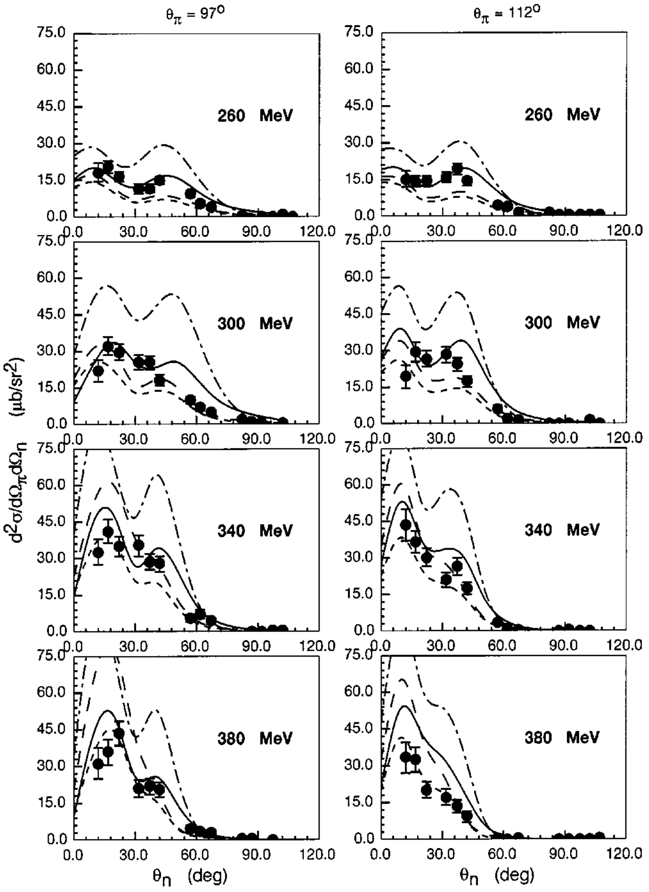

FIG. 8. As Fig. 7 for $\theta_\pi = 97°$ and 112°.

A significant difference occurs between the present ^{12}C$(\gamma,\pi^+n)^{11}$B data and the earlier ^{16}O$(\gamma,\pi^-p)^{15}$N measurement [3] in the dependence of the cross section on θ_π. We do not observe the factor of 3 reduction in the cross section between $\theta_\pi = 120°$ and $\theta_\pi = 67°$ as reported in Ref. [3] and discussed in Ref. [23]. Since the reactions (γ,π^+n) and (γ,π^-p) on self conjugate $N = Z$ nuclei are expected to be similar from isospin arguments, it is difficult to understand how such a large difference can arise. Since the present forward and backward angle data were accumulated simultaneously using adjacent regions of common detector systems we can only assume that the ^{16}O$(\gamma,\pi^-p)^{15}$N data, which used different setups for forward and backward angles, contain a systematic error. The most recent high resolution ^{16}O$(\gamma,\pi^-p)^{15}$N experiment at $E_\gamma \sim 360$ MeV by van Uden *et al.* [4] gives a similar conclusion.

Comparison with theoretical calculations

A more quantitative assessment of our data was obtained by comparing the results to plane-wave impulse approximation (PWIA) and DWIA calculations made by Lee and Wright [24] (referred to in the following as LWPW and LWDW, respectively), and by Vanderhaeghen [25] (referred to as VPW and VDW, respectively). Both models have three basic ingredients: (1) single nucleon bound state wave functions and associated spectroscopic factors, (2) an elementary π-photoproduction operator, and (3) π and nucleon optical model potentials.

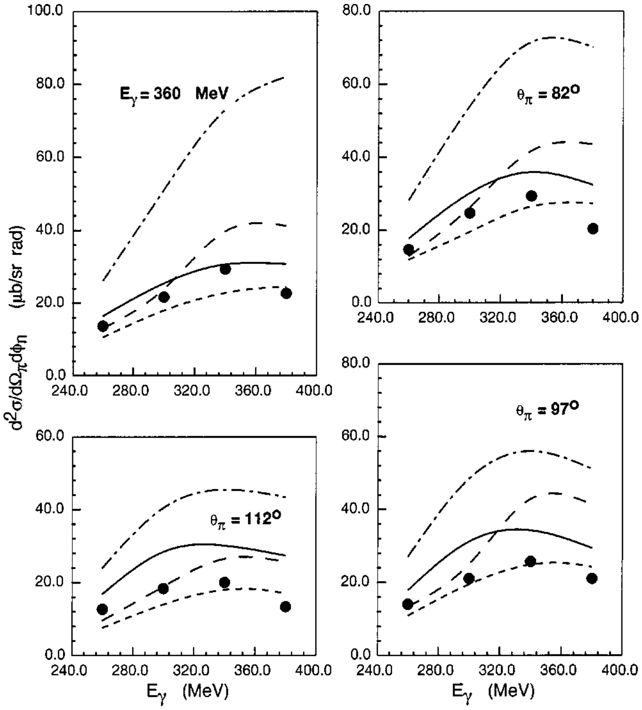

FIG. 9. Differential cross sections for the ^{12}C$(\gamma,\pi^+n)^{11}$B reaction versus photon energy. The results are integrated over E_n, E_π, and θ_n. The E_γ, θ_π, ϕ_π, and ϕ_n bins are as shown in Table I. The theory curves are as for Fig. 7.

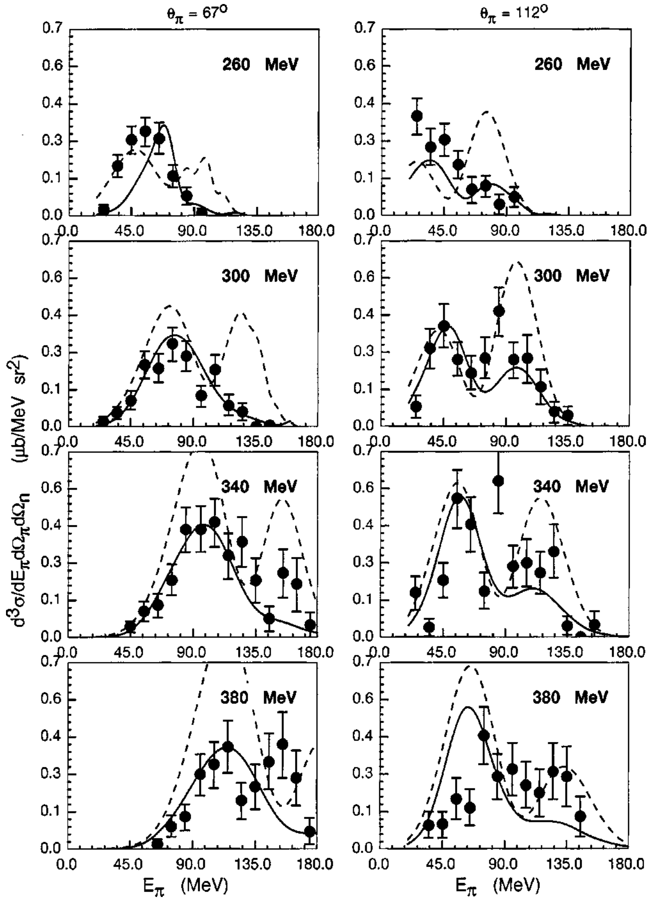

FIG. 10. Differential cross sections for the ^{12}C$(\gamma,\pi^+n)^{11}$B reaction versus π^+ kinetic energy. The θ_π and θ_n bins are 10° and 15° wide, respectively. The ϕ_π and ϕ_n bins are as shown in Table I. The results are integrated over E_n. The theory curves are LWPW (dashed) and LWDW (solid) calculations.

We first describe the calculations of Lee and Wright (LW), which were performed using the model (LWB) described by Li, Wright, and Bennhold [26]. The proton $1p_{3/2}$ bound-state was represented by a harmonic oscillator wave function, which was considered adequate for the predominantly low initial nucleon momenta involved in quasifree π production. The value used for the spectroscopic factor was $S=2.6$, which is derived from ^{12}C$(e,e'p)^{11}$B measurements [26].

For the π-photoproduction process, the full Blomqvist-Laget production operator [16,27,28] was used. The use of this phenomenological operator allows possible Δ-nuclear medium effects to be investigated by varying the mass M_Δ and the decay width Γ_Δ, as shown in LWB for selected kinematics in the Δ resonance region. Although the model also allows for the $E2/M1$ ratio in the $N\rightarrow\Delta$ transition to be varied, changes in cross sections brought about by varying this ratio are much smaller than those produced by changing M_Δ and Γ_Δ [26].

The π optical model used was developed by Stricker, McManus, and Carr based on a solution of the Klein-Gordon equation [29]. Their analyses of low energy data give good agreement with pionic atom results, nuclear absorption and π-nucleus scattering cross sections. An extension of the optical model parameters up to $E_\pi=220$ MeV, which covers the range of E_π observed in our measurements, is known to give satisfactory agreement with a broad range of data [26]. The n optical potential used was the global phenomenological potential of Schwand *et al.* [30].

The Vanderhaeghen results (*V*) were obtained using Hartree-Fock-Skyrme wave functions to describe the $1p_{3/2}$ bound state [25]. As for the LW calculations, a spectroscopic factor of $S=2.6$ was used. The elementary π-photoproduction operator was derived from a fully relativistic and unitary model developed by Vanderhaeghen [25]. This was tested successfully on an extensive data set, which included both unpolarized and polarized photoproduction observables, and both charged and neutral π production. For the ^{12}C$(\gamma,\pi^+n)^{11}$B calculations, Δ-medium effects derived by Oset *et al.* [31] were included.

The outgoing π wave function was calculated using an effective description based on the results of Stricker, McManus, and Carr [29], Seki *et al.* [32], and Nieves *et al.* [33] for $E_\pi \leqslant 50$ MeV, and Cottingame *et al.* [34], and Gmitro *et al.* [35], for $E_\pi=50$–120 MeV. The method used is analagous to the approach followed by Bergstrom [36] for the ^{12}C$(\gamma,\pi^0)^{12}$C reaction. At very low energies, the pionic atom values were recovered and the model was able to describe in a reasonable way both π^+ and π^- scattering on ^{12}C in the range $E_\pi=50$–120 MeV [25]. However, uncertainties in the description become larger at energies $E_\pi \geqslant 120$ MeV [25].

For the VDW calculations, the outgoing nucleon wave function was determined using the optical potentials for ^{12}C taken from Schwand *et al.* [30] and Meyer *et al.* [37]. It was checked that the p-nucleus observables in the kinetic energy range $E_p = 80\text{–}200$ MeV are fairly accurately reproduced by this potential.

The main difference between the two sets of calculations is the absence of Δ-medium effects in LW. Although these effects could have been simulated in LW by varying M_Δ and Γ_Δ, this was not carried out due to the large computer time requirement. Another difference is that the *V* calculations used an unfactorized (nonlocal potential) DWIA formalism as opposed to the local potential DWIA approach [26] of the LW calculations. In this way the *V* calculations retain off-shell effects in the intermediate state, such that the nucleon and π are not restricted to their asymptotic momenta before undergoing FSI. As a result, the unfactorized calculations in general yield a higher cross section. The cross section difference between the local and nonlocal DWIA calculations is expected to be typically $\pm 10\%$ [24,4]. Neither the LW nor *V* models include the decay channel $\Delta + N \rightarrow N + N$, which is allowed in the medium and will tend to reduce the quasifree cross section. The effect of this decay is however expected to be small at the E_γ energies considered here [24].

For comparison with the data, the calculations are averaged over the detector acceptances given in Table I. When making these comparisons, we note that only the statistical errors in the experimental results need to be taken into account since they are normalized to the same $p(\gamma,\pi^+ n)$ data which was fitted to obtain the elementary π-photoproduction operators used in the calculations. The main uncertainties in the calculations are undoubtedly associated with the optical model estimates of the FSI. In considering this, we note that for both sets of calculations, the DWIA results are approximately a factor of 2 lower than the PWIA results, which indicates that $\sim 50\%$ of the quasifree events involving $1p$ shell nucleons are removed to higher missing energies by FSI. A comparison of *n* FSI obtained [15,6] by using two sets of optical model parameters (Abdul-Jalil and Jackson [38] and Nadasen *et al.* [39]) with the code THREEDEE [40] indicated that the calculated effects of *n* scattering and absorption could be uncertain by up to $\pm 20\%$ for $E_\gamma \sim 260$ MeV. At energies $E_\gamma \sim 360$ MeV, appropriate to Δ excitation and where the *n* absorption is much lower, this uncertainty became $\pm 3\%$. However, the π FSI increase with E_γ and the π optical model parameters also have uncertainties associated with them. In view of this, we estimate an overall uncertainty in the DWIA results due to the optical model parameters used of $\pm 15\%$. In the case of the LWDW results, there is an additional uncertainty of $\pm 10\%$ to be taken into account due to the use of the local potential approximation.

Reasonable qualitative agreement in shape between the DW calculations and the data is obtained for all the results shown in Figs. 7–8, which adds further weight to the assumption that in our kinematic regime, the $^{12}\mathrm{C}(\gamma,\pi^+ n)^{11}\mathrm{B}$ reaction proceeds through a quasifree π-production mechanism. It is interesting to note that on average the VDW curves are in closest agreement with the measured cross sections, whereas the LWDW curves tend to lie above the data. Additional support for this observation is given by the integrated results shown in Fig. 9, which have a higher statistical accuracy. Although these results are qualitatively as expected if Δ-medium effects are present, it is not possible at this time to conclude that Δ-medium effects have been observed due to the uncertainties in the absolute normalization of the data and the theoretical calulations, in particular the treatment of FSI. Clearly, a quantitative estimate of the magnitude of Δ-medium effects will require more acurate data and a more detailed theoretical treatment.

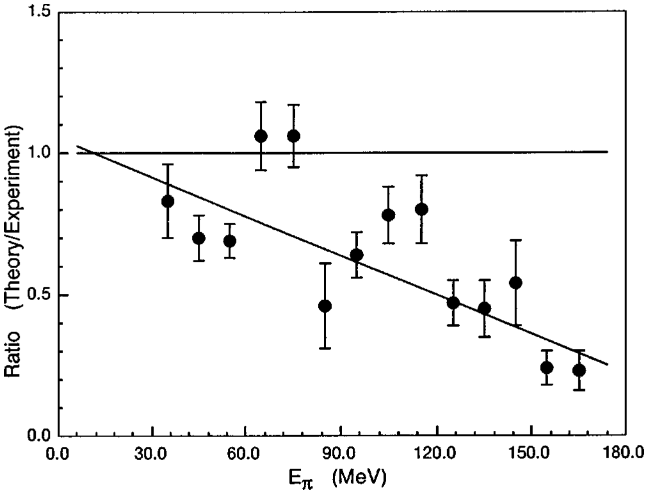

FIG. 11. Ratio of (LWDW theory/experiment) versus E_π derived from the results shown in Fig. 10.

To consider the LWDW results further, we note that the calculated curves shown in Fig. 9 lie 10–100 % above the data, the largest differences occuring at the largest θ_π. Calculations shown in LWB for the $^{16}\mathrm{O}(\gamma,\pi^- p)^{15}\mathrm{N}$ reaction indicate that a reduction in M_Δ by $\sim 2-3\ \%$, which they consider to be the appropriate amount to simulate the Δ-medium effects, reduces the cross section on average by $\sim 30\%$. However, the largest reduction ($\sim 40\%$) occurs at forward angles close to $\theta_\pi = 67°$ with smaller effects ($\sim 20\%$) occuring at large angles, such as $\theta_\pi = 112°$. A similar reduction in M_Δ would therefore improve the agreement between LWDW and the present data on average, but large discrepancies would remain at $\theta_\pi = 67°$ and 112°. A possible explanation in terms of the π and *n* optical potentials is given below.

A comparison of the theory to the E_π dependence of the differential cross section, shown in Fig. 10, suggests that the optical potentials used in the calculations may need to be modified. Overall, the LWPW and LWDW curves describe the shapes of the spectra quite well, in particular the tendency towards a double humped shape, which is seen as a consequence of the $1p$ wave function of the knocked out *p*, provided that the effect of distortion is not too large. However, there is some evidence that the LWDW theory underestimates the data at the higher E_π. To investigate this, the weighted mean of the ratio, R = theory/experiment, is plotted as a function of E_π in Fig. 11 together with a straight line fit. Based on this line, we conclude that the attenuation of the π, *n*, or both outgoing waves has the wrong energy dependence and may overestimate the flux losses for high values of E_π, which also correspond to low E_n. In both cases this is the energy region where the absorption is highest. This offers a possible solution of the problem discussed above. Since, on average, forward emitted pions have higher energies, the effect of using π and n optical model potentials that are too absorptive is to reduce the calculated cross sections more at forward than backward θ_π. This suggests that a justifiable reduction of M_Δ in conjunction with less absorptive optical potentials could lead to acceptable fits to all of the data shown in Figs. 7–10.

CONCLUSION

Data of good statistical accuracy have been obtained for the $^{12}\mathrm{C}(\gamma,\pi^+n)^{11}\mathrm{B}$ reaction over a wide range of E_γ, θ_π, and θ_n using large solid-angle plastic scintillator arrays in coincidence with a tagged photon spectrometer. The missing energy resolution obtained was sufficiently good to resolve events due to the removal of $1p$-shell protons from events involving the $1s$ shell or those in which strong FSI reduces E_π or E_n. A comparison of DWIA calculations to the $1p$-shell data is consistent with the explanation that modifications to the amplitudes describing Δ excitation, propagation, and decay may be occuring in the nuclear medium. A comparison of the LWDW results with the E_π dependence of the differential cross sections suggests that the optical model parameters used in both sets of DWIA calculations lead to an overestimate of the loss of π and n flux at high E_π and low E_n, respectively. Clearly, the interpretation of these results would benefit from a more careful and detailed theoretical investigation. In the future, we plan to investigate more targets using the present detector system and to include asymmetry measurements with polarized photons.

ACKNOWLEDGMENTS

This work was supported by grants from the U.K. EPSRC, the British Council, the DFG (Mu705/3), BMFT (06Tü 656), DAAD (313-ARC-VI-92/118), the EC [SCI.0910C(JR)], and NATO (CRG 920171, CRG 970268). The authors wish to thank the Institute für Kernphysik of the University of Mainz for the use of its facilities and assistance during the experiment. Five of us (J.A.M., G.E.C., D.G.J., D.P.W., and T.T.Y.) are grateful to the EPSRC for financial support.

[1] R. Carrasco and E. Oset, Nucl. Phys. **A536**, 445 (1992); R. Carrasco, E. Oset, and L. L. Salcedo, Nucl. Phys. **A541**, 585 (1992); R. Carrasco, M. J. Vicente Vacas, and E. Oset, Nucl. Phys. **A570**, 701 (1994).
[2] I. V. Glavanokov, Yad Fiz. **29**, 1455 (1979) [Sov. J. Nucl. Phys. **29**, 746 (1979)].
[3] L. D. Pham *et al.*, Phys. Rev. C **46**, 621 (1992).
[4] M. A. van Uden *et al.*, Phys. Rev. C **58**, 3462 (1998).
[5] K. Hicks *et al.*, Phys. Rev. C **55**, R12 (1997).
[6] J. A. MacKenzie *et al.*, Phys. Rev. C **54**, R6 (1996).
[7] I. Anthony *et al.*, Nucl. Instrum. Methods Phys. Res. A **301**, 230 (1991).
[8] S. J. Hall *et al.*, Nucl. Instrum. Methods Phys. Res. A **368**, 698 (1996).
[9] I. J. D. MacGregor *et al.*, Nucl. Instrum. Methods Phys. Res. A **382**, 479 (1996).
[10] P. Grabmayr *et al.*, Nucl. Instrum. Methods Phys. Res. A **402**, 85 (1998).
[11] J. R. M. Annand and B. Oussena, Nucl. Instrum. Methods Phys. Res. A **330**, 220 (1993); J. R. M. Annand, I. Anthony, and B. Oussena, *ibid.* **368**, 385 (1996).
[12] R. Brun, M. Hansroul, and J. C. Lassalle, GEANT User's Guide, DD/EE/82 CERN (1982).
[13] G. E. Cross *et al.*, Nucl. Phys. **A593**, 463 (1995).
[14] R. A. Cecil *et al.*, Nucl. Instrum. Methods **161**, 439 (1979).
[15] J. A. Mackenzie, Ph.D. thesis, Edinburgh University, 1995 (unpublished).
[16] I. Blomqvist and J. M. Laget, Nucl. Phys. **A280**, 405 (1977).
[17] C. Betourne *et al.*, Phys. Rev. **172**, 1343 (1968).
[18] J. Mougey *et al.*, Nucl. Phys. **A262**, 461 (1976).
[19] S. L. Belostotskii *et al.*, Yad Fiz. **41**, 1425 (1985) [Sov. J. Nucl. Phys. **41**, 903 (1985)]; Y. V. Dotsenko and V. E. Starodubskii, *ibid.* **42**, 66 (1985).
[20] M. Benjamintz *et al.*, Phys. Rev. C **58**, 964 (1998).
[21] G. van der Steenhoven *et al.*, Nucl. Phys. **A480**, 547 (1988); **A484**, 445 (1988).
[22] J. F. Arneil, Ph.D. thesis, Edinburgh University, 1998 (unpublished).
[23] T. Sato and T. Takaki, Nucl. Phys. **A562**, 673 (1993).
[24] F. X. Lee and L. E. Wright, Calculations carried out specifically for inclusion in this paper.
[25] M. Vanderhaeghen (private communication), Ph.D. thesis, University of Utrecht, The Netherlands, 1995.
[26] X. Li, L. E. Wright, and C. Bennhold, Phys. Rev. C **48**, 816 (1993).
[27] J. M. Laget, Nucl. Phys. **A481**, 765 (1987).
[28] R. M. Davidson, N. C. Mukhopadhyay, and R. S. Wittman, Phys. Rev. Lett. **56**, 804 (1986).
[29] K. Stricker, H. McManus, and J. A. Carr, Phys. Rev. C **19**, 929 (1979); **22**, 2043 (1980); **25**, 952 (1982).
[30] P. Schwand *et al.*, Phys. Rev. C **26**, 55 (1982).
[31] E. Oset *et al.*, Nucl. Phys. **A588**, 819 (1995).
[32] P. Seki, K. Masutani, and K. Yazaki, Phys. Rev. C **27**, 2817 (1983).
[33] J. Nieves *et al.*, Nucl. Phys. **A554**, 554 (1993).
[34] W. B. Cottingame and D. B. Holtkamp, Phys. Rev. Lett. **45**, 1828 (1980).
[35] N. Gmitro *et al.*, Yad. Fiz. **40**, 107 (1984) [Sov. J. Nucl. Phys. **40**, 68 (1984)].
[36] J. Bergstrom, Phys. Rev. C **50**, 2979 (1994).
[37] H. O. Meyer *et al.*, Phys. Rev. C **27**, 2817 (1983).
[38] I. Abdul-Jalil and Daphne F. Jackson, J. Phys. G **5**, 1699 (1979).
[39] A. Nadasen *et al.*, Phys. Rev. C **23**, 1023 (1981).
[40] N. S. Chant and P. G. Roos, Phys. Rev. C **15**, 57 (1977).